Anisotropic ordering in sheared binary fluids with viscous asymmetry: Experiment and computer simulation

H. S. Jeon,[1,*] Z. Shou,[2,†] A. Chakrabarti,[2] and E. K. Hobbie[1]
[1]*National Institute of Standards and Technology, Gaithersburg, Maryland 20899*
[2]*Department of Physics, Kansas State University, Manhattan, Kansas 66506*
(Received 7 January 2002; published 11 April 2002)

Optical measurements of the structure and morphology of phase-separating polymer blend under simple shear flow have been performed and the results are compared with computer simulations of sheared phase-separating binary mixtures with viscous asymmetry in the fluid components. Information about the structure is obtained from the two-point composition correlation function. Both experiment and simulation suggest subtle differences in the shear response depending on whether the more viscous phase is dispersed or continuous. Measurements of the string width along the neutral direction suggest power-law decay in the shear rate with an exponent of 1/3 when the more viscous phase is dispersed. The simulations suggest that the mean string width, measured along the velocity-gradient direction in the two-dimensional model calculation, exhibits power-law decay in the shear rate with an exponent of 1/3 independent of which phase is dispersed.

DOI: 10.1103/PhysRevE.65.041508 PACS number(s): 83.50.Ax, 47.55.Dz, 83.80.Tc

I. INTRODUCTION

The effect of shear flow on a phase-separating binary fluid in the vicinity of a critical point of unmixing is of great practical importance in the processing of immiscible fluids, where flows that resemble simple shear are often used to emulsify or mix immiscible components. In such applications, it may often be the case that the constituents of a multiphase complex fluid exhibit profound differences in their rheological properties, such as viscosity and elasticity. A particularly important example of this is encountered in the processing of polymer blends, where asymmetry in the viscoelasticity of the components is common. Past experimental [1–3] and computational [4,5] studies have investigated the effect of simple shear flow on the morphology of phase-separating binary fluids and polymer blends. The scenario in which there is asymmetry in the viscosity of two essentially Newtonian fluid components, however, has received limited attention [6,7].

When subjected to shear flow, a phase-separating binary fluid will exhibit distinct steady-state, anisotropic domain patterns as the shear rate increases with respect to the characteristic relaxation rate of the quiescent spinodal instability. In the limit of very weak shear, the flow stabilizes the instability, leading to a domain pattern with limited anisotropy, often taking the form of an emulsionlike distribution of moderately deformed, nearly spherical droplets. As the shear rate ($\dot{\gamma}$) increases, the stabilized domains deform and rupture. The mixing effect of the shear field leads to a reduced interfacial tension very close to criticality, where the steady-state domain pattern becomes highly elongated along the direction of flow [1–5], and at sufficiently high shear rates the mixture becomes homogeneous. In most past studies, the two components are assumed to have equal viscosities. For mixtures whose pure components exhibit viscous asymmetry, the assumption that the viscosities are comparable may have some validity as a leading-order approximation close to the critical point in the regime of strong shear, where the mixture is approaching a homogenized state. In a number of cases of practical interest, however, this may not be the case, and a higher degree of accuracy is desired. Viscous asymmetry is an important variable, for example, in the stability of cylindrical filaments under shear [8].

In this paper, optical measurements of the structure and morphology of phase-separating polymer blend under simple shear flow have been performed and the results are compared with computer simulations of sheared phase-separating binary mixtures with viscous asymmetry in the fluid components. Information about the structure is obtained from the two-point composition correlation function. Both experiment and simulation suggest subtle differences in the shear response depending on whether the more viscous phase is dispersed or continuous. Measurements of the string width along the neutral direction suggest power-law decay in the shear rate with an exponent of 1/3 when the more viscous phase is dispersed, but suggest an enhanced width when the less viscous phase is dispersed. The simulations, which are carried out in two dimensions, suggest that the mean string width, measured along the velocity-gradient direction, exhibits power-law decay in the shear rate with an exponent of 1/3 independent of which phase is dispersed.

II. EXPERIMENT

The details of the binary polymer mixture, the instrument, the phase diagram, and the rheology are described in detail elsewhere [6], and here we just give a brief description. The blends are mixtures of polyisoprene (PI) and polybutadiene (PB), where the shear viscosity of the PI and PB are 6.67×10^3 and 2.35×10^3 P, respectively. The PI volume

*Present address: Department of Petroleum and Chemical Engineering, New Mexico Institute of Mining and Technology, Socorro, New Mexico 87801.

†Present address: Department of Chemical Engineering, University of Pittsburgh, Pittsburgh, Pennsylvania 15260.

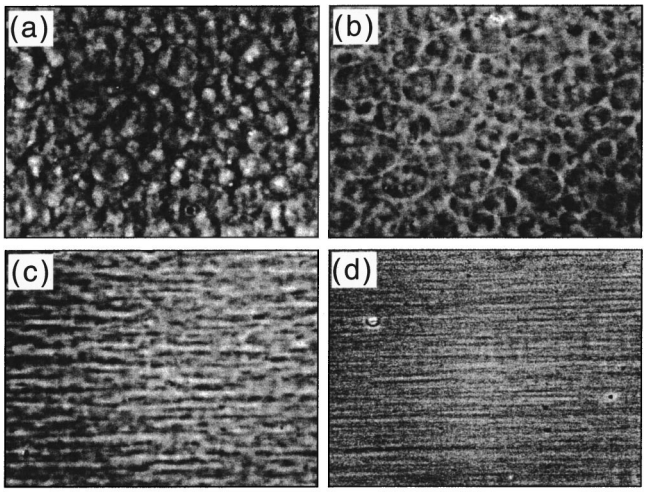

FIG. 1. Optical micrographs at different shear rates for a PI volume fraction of $\phi=0.40$ (40-60 blend), where the width of each micrograph is 200 μm. The droplets are PI rich in a PB-rich matrix, at (a) 0.001, (b) 0.01, (c) 0.1, and (d) 10 s^{-1}. The flow direction is to the right and the gradient direction is into the page. The ratio of the droplet to matrix viscosity is around 2.67.

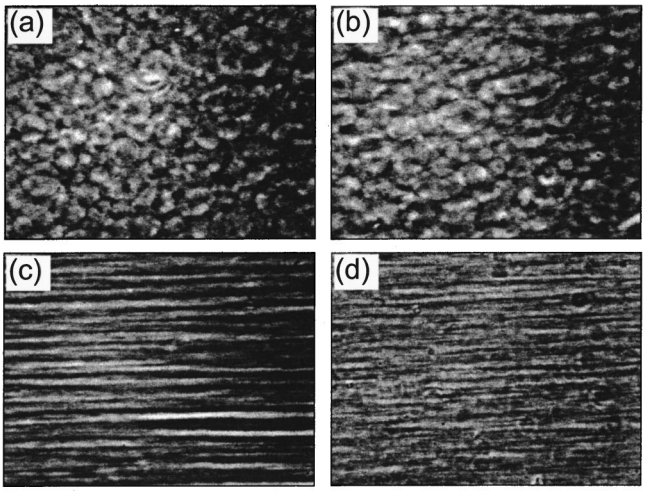

FIG. 2. Optical micrographs at different shear rates for a PI volume fraction of $\phi=0.60$ (60-40 blend), where the width of each micrograph is 200 μm. The droplets are PB rich in a PI-rich matrix, at (a) 0.001, (b) 0.01, (c) 0.1, and (d) 10 s^{-1}. The flow direction is to the right and the gradient direction is into the page. The ratio of the droplet to matrix viscosity is around 0.37.

fraction is denoted ϕ, and we consider the response of two mixtures, $\phi=0.40$ and 0.60. The mixtures exhibit lower-critical-solution-temperature behavior and phase separate upon heating, with a critical composition and temperature of $\phi_c=0.43$ and $T_c=(61.5\pm0.5)\,^{\circ}$C. For $\phi<0.55$, the quiescent viscosity ratio is $\lambda=2.67$, while for $\phi>0.55$, $\lambda=0.37$ [6]. Neither component exhibits any shear thinning in the viscosity as a function of shear rate. The optical measurements were carried out as a function of shear rate at 130 °C, which corresponds to quench depths of $\Delta T=70$ and 65 K for $\phi=0.40$ and 0.60, respectively. In a reduced temperature scheme ($\Delta T/T_s$) these quench depths are 0.21 and 0.19, respectively. In all of the measurements, the samples were heated from room temperature to 130 °C and annealed for 2 h before shearing. The shear rate was then stepped up incrementally.

Optical micrographs at different shear rates for a PI volume fraction $\phi=0.40$ (40-60 blend) are shown in Fig. 1. The droplets are PI rich in a PB-rich matrix, and the quiescent ratio of the droplet to matrix viscosity is around 2.67. The width of each micrograph is 200 μm, the flow direction is to the right, and the gradient direction is into the page. At this composition, which is close to critical, the morphology has coarsened into well-defined PI-rich droplets in a PB-rich matrix before the shear is applied. At $\dot{\gamma}=0.001\ s^{-1}$, the coarsening of the domains is stabilized by the shear flow, and the steady-state morphology is emulsionlike, with a polydisperse distribution of essentially spherical droplets [Fig. 1(a)]. At $\dot{\gamma}=0.01\ s^{-1}$, the flow starts to deform the droplets so that the projection into the flow-vorticity plane becomes extended along the flow direction [Fig. 1(b)]. At $\dot{\gamma}=0.1\ s^{-1}$, the droplets have started to burst and the anisotropy has become more pronounced. A stringlike pattern with a high aspect ratio has emerged at $\dot{\gamma}=10\ s^{-1}$ [Fig. 1(d)].

Optical micrographs at different shear rates for a PI volume fraction $\phi=0.60$ (60-40 blend) are shown in Fig. 2, where again the width of each micrograph is 200 μm. The droplets are PB rich in a PI-rich matrix, and the ratio of the droplet to matrix viscosity is around 0.37. The overall evolution of the anisotropy is qualitatively quite similar to that exhibited at $\phi=0.40$, however, the steady-state morphology at higher shear rates [Figs. 2(c) and 2(d)] is coarser, which can be most easily seen by comparing Figs. 1(c) and 2(c). The origin of this difference probably lies in the viscous asymmetry of the two components. For isolated droplets, filamentlike structures generally do not occur in shear flow for $\lambda>1$, while for $\lambda<1$ they do [9]. Thus, the domains in Fig. 2 are readily extended to high aspect ratios at shear rates where those shown in Fig. 1 tend to rupture. The appearance of a stringlike pattern at high shear rates when the viscosity ratio is greater than or comparable to unity has been previously attributed to a shear-induced decrease in the interfacial tension due to the homogenizing effect of the shear flow [1]. Shear-induced coalescence, however, clearly plays an equally important role, particularly in mixtures with significantly different melt viscosities for which $\lambda<1$.

By thresholding the optical micrograph into a black and white binary image, we obtain an approximate representation of the two-phase domain structure [10]. From this, we compute the two-point composition correlation function, $g(\mathbf{r})$, which can then be projected onto the flow (x) and vorticity (z) directions. A measure of the domain dimensions along the flow and vorticity directions can then be obtained from these projections as a function of shear rate. Along both axes, the data were fit to the expression $g(x_i)\approx\exp(-2x_i/R_i)$ to obtain the length scales R_x and R_z [11]. Figure 3 shows the projected correlation functions as a function of shear rate for $\phi=0.40$ along (a) the vorticity direction and (b) the flow direction. The insets show the two length scales as a function

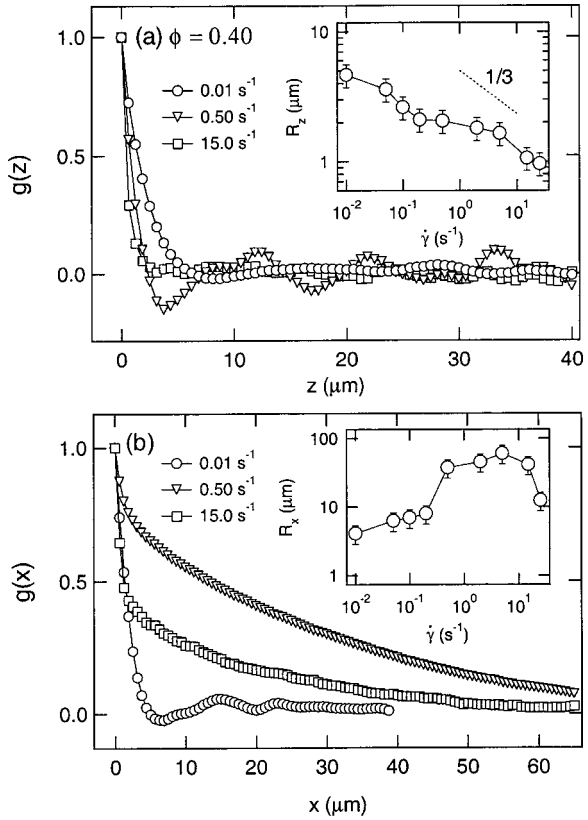

FIG. 3. Two-point correlation functions computed for the data in Fig. 1 along (a) the vorticity direction, and (b) along the flow direction. The insets show the characteristic length scale for each direction as a function of shear rate, where R_z and R_x have been determined as described in the text. Power-law decay with an exponent of 1/3 is shown as a dashed line in (a).

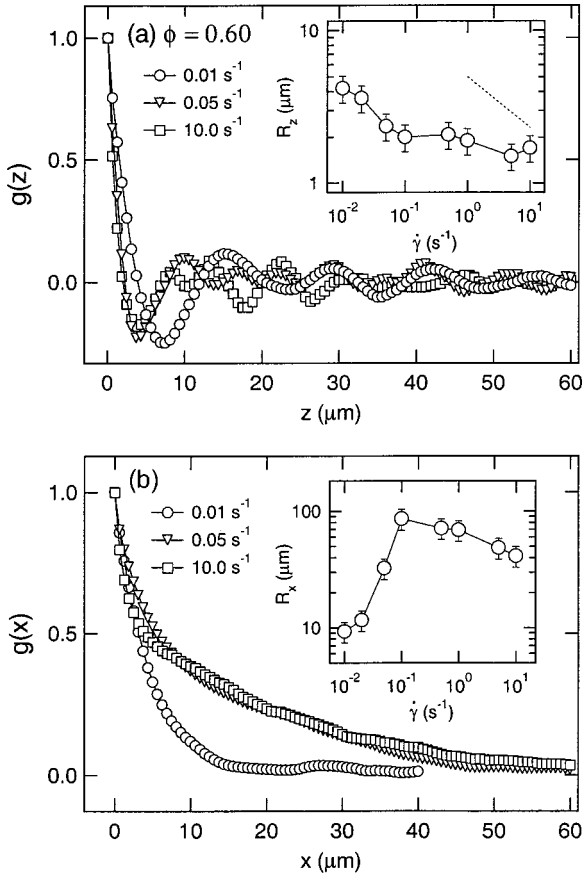

FIG. 4. Two-point correlation functions computed for the data in Fig. 2 along (a) the vorticity direction, and (b) along the flow direction. The insets show the characteristic length scales along these directions as a function of shear rate. Power-law decay with an exponent of 1/3 is shown as a dashed line in (a).

of shear rate. Figure 4 shows an analogous plot for $\phi=0.60$. For $\phi=0.40$, the string width in the vorticity direction, R_z, exhibits an asymptotic power-law decay in the shear rate with an exponent of 1/3, while for $\phi=0.60$ the width appears to level off as the shear rate increases. Similarly, the coherence length along the flow direction, R_x, is slightly larger for $\phi=0.60$ over a comparable range of shear rates. The difference in length scale along the vorticity direction might indicate a tendency for the droplets to be more easily flattened into ribbonlike shapes when the droplets are less viscous than the continuous phase ($\phi=0.60$). The difference along the flow direction might reflect droplets that are more viscous than the matrix ($\phi=0.40$) being more resistant to the deformation imposed by the shear.

III. SIMULATION

We consider an *A*-*B* binary viscous liquid mixture quenched rapidly into the two-phase region in the presence of a uniform shear flow. The system is characterized by an order parameter $\phi(\mathbf{r},t)$, which is the difference of local concentrations of the *A* component and the *B* component. The *A* and *B* components of the mixture have viscosity η_A and η_B, respectively. For simplicity, the effective viscosity of the mixture, η, is considered to take the linear form [12]

$$\eta(\phi)=\frac{\eta_A+\eta_B}{2}+\frac{\eta_A-\eta_B}{2}\phi. \tag{1}$$

In Eq. (1), η becomes η_A as ϕ approaches $+1$, which corresponds to *A*-rich case. On the other hand, η becomes η_B in the pure *B* phase (when ϕ approaches -1). The dynamics of phase separation in a binary liquid mixture can be described theoretically within the model-*H* formalism of Hohenberg and Halperin [13], which consists of a modified Cahn-Hilliard equation [14] along with a Navier-Stokes type equation and an incompressibility condition on the fluid velocity **u**;

$$\frac{\partial\phi}{\partial t}+\mathbf{u}\cdot\nabla\phi=\nabla^2\frac{\delta F}{\delta\phi}+\zeta, \tag{2}$$

$$\rho\left(\frac{\partial\mathbf{u}}{\partial t}+\mathbf{u}\cdot\nabla\mathbf{u}\right)=\nabla\cdot[\eta(\phi)\overline{\mathbf{T}}]-\phi\nabla\frac{\delta F}{\delta\phi}-\nabla P, \tag{3}$$

$$\nabla\cdot\mathbf{u}=0. \tag{4}$$

Here, the rate-of-strain tensor $\overline{\mathbf{T}}$ has the following components:

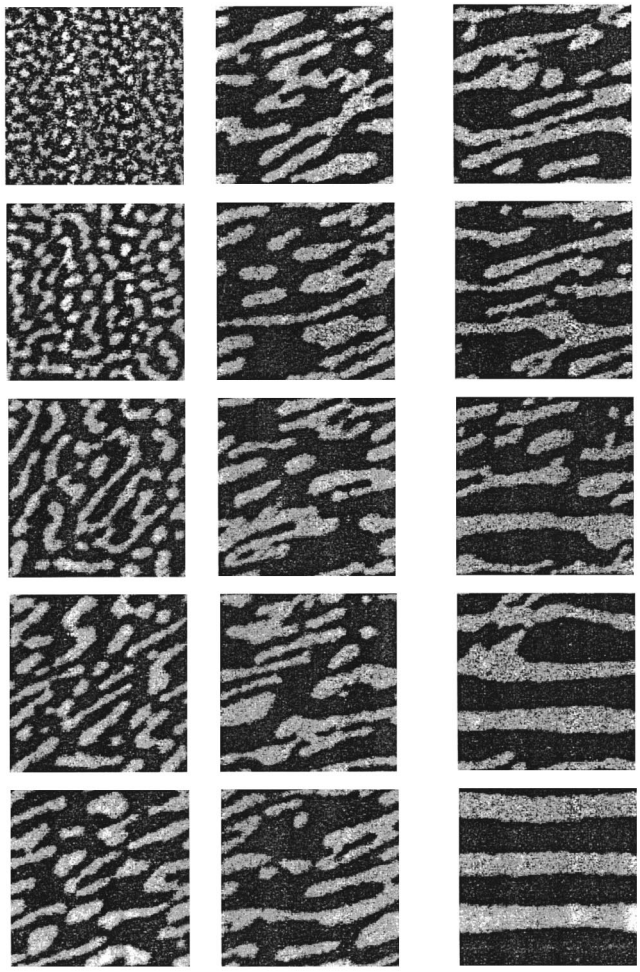

FIG. 5. Typical snapshots of the simulated concentration profile of the system at various times after the quench for a 40-60 *A-B* mixture, respectively, with a rescaled shear rate $\dot{\gamma}=0.032$. Time after the quench increases from the left corner down. The snapshots are shown at rescaled times 0.4, 1, 2, 3, 5, 7, 9, 11, 13, 15, 17, 19, 30, 60, and 120, respectively.

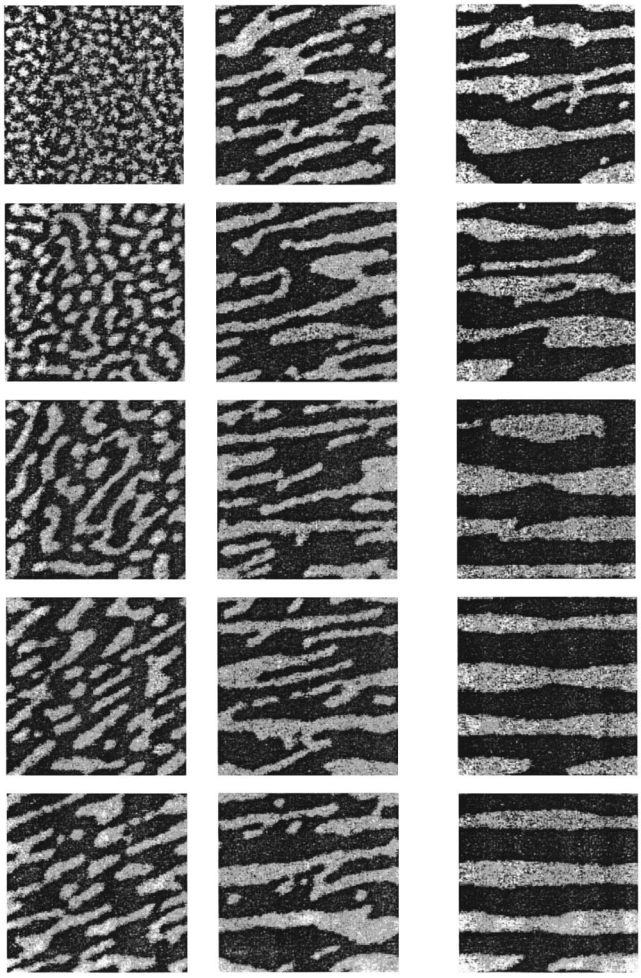

FIG. 6. Typical snapshots of the simulated concentration profile of the system at various times after the quench for a 60-40 *A-B* mixture, respectively, with a rescaled shear rate $\dot{\gamma}=0.032$. The snapshots are shown at the same rescaled times as in Fig. 5.

$$\overline{\mathbf{T}}_{ij}=\frac{\partial u_i}{\partial x_j}+\frac{\partial u_j}{\partial x_i}. \tag{5}$$

The noise term $\zeta(\mathbf{r},t)$ is Gaussian distributed with correlations

$$\langle \zeta(\mathbf{r},t)\rangle=0, \tag{6}$$

$$\langle \zeta(\mathbf{r},t)\zeta(\mathbf{r}',t')\rangle=-\varepsilon\nabla^2\delta(\mathbf{r}-\mathbf{r}')\,\delta(t-t'), \tag{7}$$

where the strength ε is proportional to the final temperature of the quench. The free energy functional representing the binary liquid mixture, $F[\phi]$, is of the conventional Ginzburg-Landau form. In the presence of an externally applied steady shear flow in the $\hat{\mathbf{x}}$ direction, the velocity field can be formally written as

$$\mathbf{u}(\mathbf{r})=\dot{\gamma}y\hat{\mathbf{x}}+\mathbf{v}(\mathbf{r}), \tag{8}$$

where $\dot{\gamma}$ is the shear rate and $\mathbf{v}(\mathbf{r})$ is the fluctuating part of the flow field.

The dynamical equations described above are numerically integrated in two-dimensional systems of sizes 128×128 and 256×256 with mesh sizes $\Delta x=\Delta y=1$ and a time step $\Delta t=0.01$. The order parameter equation is integrated via a straightforward Euler method, while the velocity equations are integrated using a fast Fourier transform method [15]. Time is measured in units of τ_ϕ, the bare characteristic diffusion time for the order parameter in Eq. (2), and distance is measured in units of ξ, the thermal correlation length. The shear rates quoted for the simulation results have units of $1/\tau_\phi$. This time scale is ''bare'' in the sense that it comes from Eq. (2) without any coupling to Eq. (3) and thus does not include viscous asymmetry. In the numerical study, we have used a technique involving a staggered mesh method [16] to satisfy the incompressibility condition. In this method, one stores the pressure P and the order parameter ϕ at the center of the cell while the velocities are stored at the midpoint of the sides. The incompressibility condition can then be enforced in a natural way. In the sheared state, the boundary condition becomes

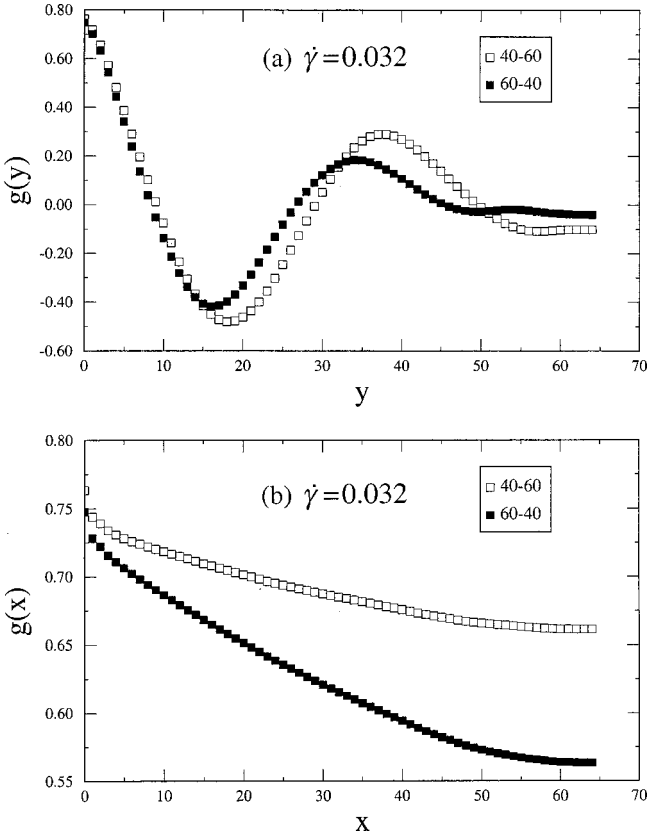

FIG. 7. (a) The correlation function $g(\mathbf{r})$ computed from the simulations projected along the gradient (y) direction in the steady state at a shear rate of 0.032 for the 40-60 and 60-40 mixtures. (b) The correlation function $g(\mathbf{r})$ projected along the flow (x) direction in the steady state at a shear rate of 0.032 for the 40-60 and 60-40 mixtures.

$$\psi(x,y,t)=\psi(x+N_xL+\dot{\gamma}tN_yL,y+N_yL,t), \tag{9}$$

where $\psi\equiv(\phi,u_x,u_y)$. The computational lattice deforms in accordance with the externally applied steady shear flow. The following transformation

$$x'=x-\dot{\gamma}ty, \quad y'=y, \quad t'=t, \tag{10}$$

is employed to permit the use of periodic boundary conditions in new coordinate directions. Accordingly, the following set of differential transformations are used:

$$\nabla\rightarrow\left(\frac{\partial}{\partial x},\frac{\partial}{\partial y}-\dot{\gamma}t\frac{\partial}{\partial x}\right), \tag{11}$$

$$\frac{\partial}{\partial t}\rightarrow\frac{\partial}{\partial t}-\dot{\gamma}y\frac{\partial}{\partial y}. \tag{12}$$

The imposed shear tends to skew the computational grids with time. This would lead to numerical instability in the simulations as the equations become stiff. To avoid this, it is necessary to remesh the grid at regular intervals [17]. The remeshing procedure utilizes the periodic boundary condition in the shear direction to move the data from the skewed grid to the rectified grid. In our $L\times L$ simulation grid, at every integer interval, we proceed with the moving of data, since at this instant the skewed lattice overlaps perfectly with the rectified one. This would thus be a convenient time to move data and avoid any interpolation onto the new grid. After remeshing, the grid progresses to its initial orthogonal position and eventually continues to the skewed position, at which point remeshing becomes necessary again.

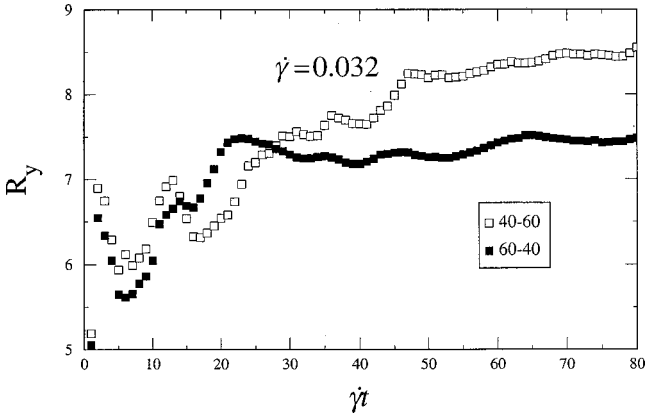

FIG. 8. The steady-state string width in the gradient direction, R_y, as a function of rescaled time after a quench to $\dot{\gamma}=0.032$ obtained from simulations of the 40-60 and 60-40 mixtures.

To compare with experimental measurements, we consider $\eta_A=3$ and $\eta_B=1$ and study domain growth in both 60-40 and 40-60 mixtures. The thermal noise strength ε is chosen to take a value of 1.2, which corresponds to a quench to a final temperature of about $0.8T_c$ in two dimensions [18]. We compute equal-time correlation functions [$g(x)$ and $g(y)$] and domain sizes [$R_x(\dot{\gamma})$ and $R_y(\dot{\gamma})$] along the flow and the gradient directions, respectively. All of these quantities are averaged over 20 initial conditions. In Figs. 5 and 6 we display typical snapshots of the concentration profile of the system at various times after the quench for a 60-40 and a 40-60 A-B mixture, respectively, with a rescaled shear rate of $\dot{\gamma}=0.032$. The time steps between snapshots in Figs. 5 and 6 are indicated in the figure captions. For early times (i.e., for $\dot{\gamma}t\leqslant 1$), the phase-separated domains are isotropic,

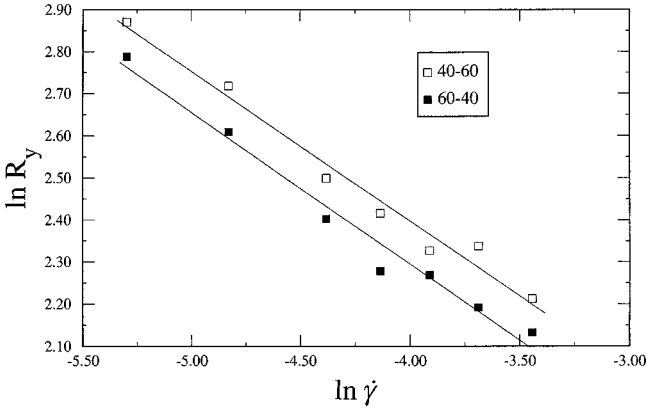

FIG. 9. The steady-state string width in the gradient direction, R_y, as a function of $\dot{\gamma}$ obtained from simulations of the 40-60 and 60-40 mixtures. The lines are power-law fits with an exponent of 1/3.

as the shear effects have yet to perturb their shape. Subsequently, the domains become elongated under the influence of the shear flow. The rupture and recombination of domains become most prominent at intermediate times ($\dot{\gamma}t \gtrsim 1$) and this leads to a maximum in the excess shear viscosity around this time. Finally, at very late times ($\dot{\gamma}t \gg 1$) lamellaelike domains form with a normal along the shear gradient ($\hat{\mathbf{y}}$) direction.

Although the snapshots for both 40-60 and 60-40 mixtures are similar, there are slight differences depending on whether the majority phase has larger viscosity (60-40) or the droplet phase has larger viscosity (40-60). Figure 7 shows the steady-state equal-time two-point composition correlation function, $g(\mathbf{r}) = \langle \phi(\mathbf{r},t)\phi(0,t)\rangle$, projected onto the gradient direction (a) and the flow direction (b) for $\dot{\gamma} = 0.032$. The late time values of the thickness of the anisotropic domains (R_y) are slightly larger for the case where droplets have a larger viscosity, although $g(x)$ exhibits a long-range decay in both mixtures. The time scale to reach a steady-state value for R_y is larger when the droplets have a larger viscosity, reflecting the ability of the more viscous domains to resist deformation imposed by the less viscous matrix (see Fig. 8). In Fig. 9 we show log-log graphs of R_y versus $\dot{\gamma}$ at the steady state. For both mixtures, $R_y \sim \dot{\gamma}^{-1/3}$, although R_y at a given shear rate is systematically larger for the case where droplets have a larger viscosity.

IV. SUMMARY AND CONCLUSIONS

We have carried out both experiments and simulations to study ordering in sheared binary liquid mixtures with viscous asymmetry. Both experiments and simulations suggest that a stringlike structure is formed under steady shear when either the droplet phase or the matrix phase has a larger viscosity. Our simulations, however, are restricted to two dimensions, which makes a direct comparison between experiment and simulation difficult. The two-dimensional simulations measure the response in the flow-gradient plane, while the experiments measure the response in the flow-vorticity plane. For $\phi = 0.40$, a comparison of R_y and R_z might be suitable, as the more viscous droplets might exhibit a tendency to be more symmetric within this plane than the less viscous droplets. Indeed, the asymptotic power-law behavior suggested by the simulations for R_y is similar to that suggested by the measurements for R_z. Simulations suggest similar power-law behavior for R_y when $\phi = 0.60$, but this was not observed in the experiments. Along the flow direction, a detailed comparison of shear response is complicated by the finite size of the simulation box.

In light of these difficulties, the best comparison between simulation and experiment perhaps can be made by considering the transient response of the simulations upon start up of shear and the transient relaxation of the measured structure upon cessation of shear. The viscous asymmetry is evident in Fig. 8 as the difference in ''equilibration'' rate. Once the shear stress has been turned on, it takes longer for the $\phi = 0.40$ case to attain a steady state. Physically, this just reflects the fact that the droplets are more viscous and thus less responsive to shear stress. The ratio of relaxation times suggested by the simulations for start up of shear for $\phi = 0.40$ and $\phi = 0.60$ (Fig. 8) is $\tau_{0.4}/\tau_{0.6} \approx 2$. Small deformation theories for isolated droplets suggest that this should be the viscosity ratio, 3 [19]. Although no simulations were carried out for cessation of shear, optical measurements show that 9 min after the shear flow has been stopped, the $\phi = 0.60$ sample still exhibits anisotropy along the direction of flow, while at the same time the $\phi = 0.40$ sample is isotropic. Physically, this suggests that the more-viscous domains are able to relax more quickly (within the less-viscous matrix) than the less-viscous domains (within the more-viscous matrix), since the latter is limited by the stress relaxation in the matrix. Our measurements suggest that the ratio of relaxation times following cessation of shear for the data described here are $\tau_{0.4}/\tau_{0.6} \approx 0.65$. Further work is needed to understand the physical origin of these ratios, but they qualitatively point toward the most profound effects of viscous asymmetry. An important distinction between experiment and simulation is that the experiments show a shear-induced homogenization to a single miscible phase at a sufficiently high shear rate, while this is not observed in the simulations. The shear-induced shift in the critical temperature has been the focus of a number of past experimental studies [1,20,21]. The simulations cannot achieve shear rates of sufficient magnitude to enter this regime, however, which is observed experimentally at around 100 s^{-1} for the mixtures described here.

ACKNOWLEDGMENTS

One of us (A.C.) would like to acknowledge The National Center of Supercomputer Applications (NCSA) for a grant of computing time and The National Institute of Standards and Technology (NIST, Gaithersburg, Maryland) for financial support of this work. E.K.H. would like to thank R. K. Hobbie for assistance with the correlation-function computer code.

[1] E. K. Hobbie, S. Kim, and C. C. Han, Phys. Rev. E **54**, R5909 (1996).
[2] T. Hashimoto, K. Matsuzaka, E. Moses, and A. Onuki, Phys. Rev. Lett. **74**, 126 (1995).
[3] L. Kielhorn, R. H. Colby, and C. C. Han, Macromolecules **33**, 2486 (2000).
[4] Z. Shou and A. Chakrabarti, Phys. Rev. E **61**, R2200 (2000).
[5] A. Onuki, Phys. Rev. A **35**, 5149 (1987).
[6] H. S. Jeon and E. K. Hobbie, Phys. Rev. E **63**, 061403 (2001).
[7] Z. Zhang, H. Zhang, and Y. Yang, J. Chem. Phys. **115**, 7783 (2001).
[8] A. Frischknecht, Phys. Rev. E **56**, 6970 (1997); **58**, 3495 (1998).
[9] J. M. Rallison, Annu. Rev. Fluid Mech. **16**, 45 (1984).
[10] E. K. Hobbie *et al.* (unpublished).
[11] This is an extension of Debye's result [P. Debye, *et al.*, J. Appl. Phys. **28**, 679 (1957)] to random anisotropic sharp interfaces [10], where R_x and R_z are correlation lengths along x and

z, respectively. The interfaces are not randomly distributed, but interactions are less important for $z \to 0$, where the fits along the *z* direction have been performed. Along the flow direction, the coherence is long range and the magnitude of *x* was not restricted in the fit. A small background has been included.

[12] N. Grizzuti, G. Buonocore, and G. Iorio, J. Rheol. **44**, 149 (2000).

[13] P. C. Hohenberg and B. I. Halperin, Rev. Mod. Phys. **49**, 435 (1977).

[14] J. D. Gunton, M. San Miguel, and P. S. Sahni, in *Phase Transition and Critical Phenomena*, edited by C. Domb and J. L. Lebowitz (Academic, London, 1983), Vol. 8.

[15] A. J. Bray, Adv. Phys. **43**, 357 (1994).

[16] J. H. Ferziger and M. Peric, *Computational Methods for Fluid Dynamics* (Springer, Berlin, 1997).

[17] M. M. Rogers, P. Moin, and W. C. Reynolds, NASA Report No. NCC-2-5 TF-25 (1986).

[18] R. Toral and A. Chakrabarti, Phys. Rev. B **42**, 2445 (1990).

[19] S. Torza, R. G. Cox, and S. G. Mason, J. Colloid Interface Sci. **38**, 395 (1972).

[20] J. Yu *et al.*, Phys. Rev. Lett. **78**, 2664 (1997).

[21] E. K. Hobbie *et al.*, Phys. Rev. Lett. **69**, 1951 (1992).